# Robust Graph Topology Inference for Multiple Brain EEG Networks

Tiziana Cattai, *Member, IEEE*, Stefania Colonnese, *Senior Member, IEEE*, and Sergio Barbarossa, *Life Fellow, IEEE*

***Abstract*—In EEG-based connectivity analysis, multiple graphs are typically available, as obtained from measurements taken under different conditions, such as frequency bands, trials, or patients' states. Identifying stable patterns of interaction among brain regions, such as functional communities, can provide valuable insight into brain organization and its changes across tasks or conditions. It is then of interest to find a method to properly combine these different graphs to obtain a clustering that is sufficiently stable and representative of brain functionalities. In this paper, we propose a method to obtain robust spectral clustering. The method relies on a statistical characterization of the multiple graphs and a small perturbation analysis of the eigen-decomposition of graphs affected by random perturbations to derive the optimal weighting that minimizes the variance of the eigenvalues. The proposed method is first tested on synthetic data, to assess its advantages with respect to conventional approaches under controllable conditions, and then it is applied to real EEG data in both healthy individuals performing motor imagery tasks and patients affected by Alzheimer's disease. The results show the ability of the method to reliably detect functional communities and quantify connectivity reorganization during cognitive tasks. Our results suggest that the proposed approach provides a valid new strategy to combine multiple graphs taking into account the statistical properties of each graph in the presence of uncertainties.**

***Index Terms*—Graph signal processing, brain EEG networks, graph inference.**

## I. Introduction

GRAPH-BASED brain functional analysis provides a quantitative and structured approach to understanding the brain's complex organization, supporting insights into normal functioning and helping develop diagnostics and treatments for various neurological and psychiatric disorders.

In this context, brain data recorded from various EEG electrodes can be modeled as signals on graph [1], [2], where the brain's structure is represented using graph models. In this context, Graph Signal Processing (GSP) techniques have been shown to facilitate the identification of network communities [3], simplify brain network representations [4], and enable tracking of mental states [5]. EEG-based approaches typically infer these interactions by employing various connectivity estimators between nodes [6], or applying the same estimator across multiple frequency bands [7]. Variations in the estimators reflect differences in assumptions, frequency bands, or noise, introducing perturbations that can affect the accuracy and consistency of the inferred brain networks.

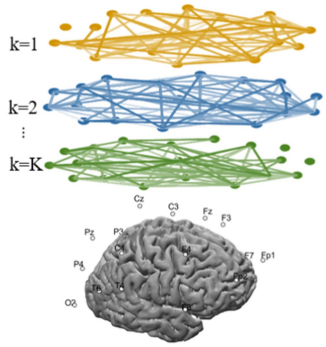


Fig. 1. Multiple brain networks of EEG signals.

This work stems from the consideration that different connectivity estimates, corresponding to distinct representations of the brain network [6] can be interpreted as multiple perturbed observations with respect to a nominal graph representing the ongoing brain activity, as shown in Fig. 1. The problem of combining multiple graph observations has been widely investigated, notably in the context of graph inference from partial observations [8], layer aggregation for spectral clustering [9], and several multiview clustering methods [10]. Our approach differs from the state-of-the-art by explicitly modeling the variability across multiple graphs as perturbations of a nominal graph and using a small perturbation analysis of the graph Laplacian eigen-decomposition to obtain a statistical model that is used to find an optimal robust combination of the features extracted from multiple graphs. The goal of this paper is to derive a robust graph topology inference algorithm that optimally combines multiple EEG-based networks considering probabilistic priors.

The integration of different graph observations, such as brain networks observed across various frequency bands, may lead to more meaningful and accurate network estimations [11].

Received 1 November 2024; revised 10 April 2025 and 14 July 2025; accepted 20 August 2025. Date of publication 10 September 2025; date of current version 15 October 2025. This work was supported by the European Union - Next Generation EU under the Italian National Recovery and Resilience Plan (NRRP), Mission 4, Component 2, Investment 1.3, CUP B53C22004050001, partnership on "Telecommunications of the Future" under Grant PE00000001 - program "RESTART". The associate editor coordinating the review of this article and approving it for publication was Dr. Dorina Thanou. *(Corresponding author: Tiziana Cattai.)*

The authors are with the Department of Information Engineering, Electronics and Telecommunications, Sapienza University of Rome, 00185 Roma, Italy (e-mail: tiziana.cattai@uniroma1.it; stefania.colonnese@uniroma1.it; sergio.barbarossa@uniroma1.it).

Digital Object Identifier 10.1109/TSIPN.2025.3606164

© 2025 The Authors. This work is licensed under a Creative Commons Attribution-NonCommercial-NoDerivatives 4.0 License. For more information, see https://creativecommons.org/licenses/by-nc-nd/4.0/

This approach also eliminates the need for time-consuming, subject-specific bandwidth tuning, which is typically required for connectivity estimation [12]. Besides, an integrated inference strategy overcomes the need to identify the subject-dependent bandwidth to be used for brain connectivity estimation, which is currently selected by a time-consuming procedure for parameter fine tuning. Furthermore, the inference can be performed using a fixed set of estimators over different subjects, facilitating the comparison of results obtained across different subjects and guaranteeing interpretable results.

In this paper, we propose a robust inference method to integrate multiple EEG observations. Firstly, we analyze how multiple connectivity estimates can serve as a statistical prior for observations. Then, we address the problem of how to combine multiple graphs. Since one of our objectives is to identify clusters of activity, we explore whether it is more effective to first combine the Laplacians of the graphs and then perform clustering, or to compute the eigenvectors of each graph separately and then combine them appropriately. One of the interesting and innovative results of this work is that the second procedure, when combined with the optimization of the combination weights, leads to a more stable result. To formulate the optimization problem, we consider each available graph as the perturbation of a nominal graph. Then, we use small perturbation analysis on the perturbations of the eigen-decomposition of the nominal graph Laplacian matrix, relying on [13]. This analysis enables us to compute the variance of the eigenvalues and eigenvectors. Starting from this statistical model, we formulate an optimization problem to find the optimal weights to combine the eigenvectors of different graphs to achieve a set of vectors to be used for spectral clustering.

We test our method on synthetic data first, to assess its performance in a controllable context. Then, we present the application of this method on two different publicly available EEG datasets, one from motor imagery-based Brain Computer Interface (BCI) experiments [14] and another with patients affected by Alzheimer's disease and healthy control subjects [15]. We show that our brain network inference, resulting from the optimal combination of the first nominal graph eigenvectors, is better than state-of-the-art methods to highlight key brain reorganization properties during different cognitive states. Specifically, the approach leads to accurate brain network metrics, such as the number of communities within the network, the association of EEG sensors with these communities, and the precise inference of the brain network structure. By properly taking into account the uncertainties in the eigenvectors responsible for spectral clustering, the proposed method leads to a robust and reliable estimation of brain connectivity.

The structure of the paper is as follows. In Section II, we present the multiple observation model and extract a perturbation prior for each observation based on the inferred connectivity. In Section III, we present our graph topology inference method and in Section IV we apply our method to real EEG-based brain functional connectivity. Finally, in Section V, we draw some conclusions.

## II. Multiple Network Observation Model

### A. Signal Observation Model

We start with the signal observation model and we present how uncertainty on the edges affects the graph observations [13]. We consider a binary undirected graph $\mathcal{G} = (\mathcal{V}, \mathcal{E})$, with a set $\mathcal{V}$ of $N$ nodes and a set $\mathcal{E}$ of $M_{\mathcal{E}}$ edges, where the $m$-th edge in $\mathcal{E}$ is associated to a pair of nodes $(m_1, m_2)$. The adjacency matrix $\mathbf{A}$ has entries $a_{m_1,m_2}$ that are 1 if $(m_1, m_2) \in \mathcal{E}$ and 0 otherwise. The diagonal matrix of node degrees $\mathbf{D}$ has entries $d_{ii} = \sum_{j=1}^{N} a_{ij}$, and the Laplacian matrix is defined as $\mathbf{L} = \mathbf{D} - \mathbf{A}$.

We remark that the binary graph $\mathcal{G}$ may either represent binary edge information or be the binarized version of a real weighted graph. Since the inference of the graph can be affected by errors, we describe the perturbation of the edge by a random variable $z_m \in \{0, 1\}$, representing the occurrence of a perturbation event on the $m$-th edge. The random variable $z_m$ is characterized as follows:

$$z_m = \begin{cases} 1, & \text{with probability } P_m \\ 0, & \text{with probability } (1 - P_m). \end{cases} \tag{1}$$

In modeling the graph, the probability $P_m$ of a perturbation event on the $m$-th edge can be a-priori known or estimated from observations. Besides, we indicate with $\sigma_m \in \{-1, 1\}$ the observed binary weight of the $m$-th graph edge. Specifically, $\sigma_m = -1$ when the link $m$ is removed from the graph or $\sigma_m = 1$ when the link is added.

Without loss of generality, we discuss the case where $P_m$ is inferred from the observations. Specifically, suppose that the graph inference assigns a weight $w_m \in [0, 1], m = 0, \cdots M_{\mathcal{E}} - 1$, to each edge and let $\mathcal{G}$ be the graph obtained by thresholding these weights, as follows:

$$A_{m_1,m_2} = \begin{cases} 1, & \text{if } w_m > \theta \\ 0, & \text{otherwise.} \end{cases} \tag{2}$$

where $m_1$ and $m_2$ the nodes linking the $m$-th edge.

This case is very common in the applications and fits the analysis carried out on real EEG data, where the use of real weighted graphs is very common. We assume that when strong or extremely weak edges are observed, i.e., when $w_m$ is close to 0 or 1, the probability of edge miss-classification due to thresholding is very small. A visual example of the steps leading to the identification of the perturbation prior appears in Fig. 2. In the followings, we will show results where the prior information $P_m$ is directly extracted from the observed network data as follows:

$$P_m \approx \begin{cases} 1 - w_m, & \text{if } w_m > \theta \\ w_m, & \text{otherwise.} \end{cases} \tag{3}$$

The rationale behind (3) is to assign a probability of perturbation to the $m$-th edge based on the reliability of the thresholding outcome. If $w_m > \theta$ (indicating a detected binary link), $P_m$ represents the false alarm probability, increasing as the weight deviates from 1; if $w_m \leq \theta$ (indicating no detected binary link), $P_m$ increases as the weight deviates from 0.

Now, since eigenvalues and eigenvectors of the Laplacian matrix play a key role in spectral clustering, we leverage the

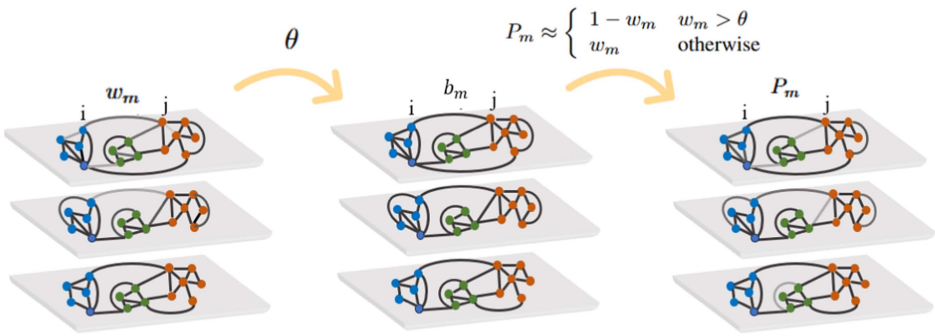


Fig. 2. Graphical representation of the proposed model for multiple K estimates of graph topology from a weighted original graph (left panel), to the binary graph after the selection of the threshold $\theta$ (central panel) and a weighted graph associated to the perturbation probability $P_m$ (right panel).

above prior knowledge of $P_m$ to derive a statistical model for the perturbations of the eigenvalues and eigenvectors of the inferred Laplacian matrix.

### B. Perturbation Analysis

With the above positions, the edges of graph $\mathcal{G}$ are characterized by their weights $w_m$, but also by a statistical prior that identifies the probability of perturbation of each edge $P_m$. Here, we exploit this twofold information and derive a probabilistic description of the perturbation expected on the Laplacian eigenstructure. Let $\mathbf{L} = \mathbf{U}\mathbf{\Lambda}\mathbf{U}^\top$ be the eigen-decomposition of $\mathbf{L}$. Uncertainty in the graph topology leads to a mismatch between the nominal Laplacian $\mathbf{L}$ and the actual observed Laplacian $\tilde{\mathbf{L}}$. The perturbation impacts the observed Laplacian by altering the eigenvectors and eigenvalues, expressed as:

$$\tilde{\mathbf{L}} = \tilde{\mathbf{U}}\tilde{\mathbf{\Lambda}}\tilde{\mathbf{U}}^\top$$

where $\tilde{\mathbf{U}}$ and $\tilde{\mathbf{\Lambda}}$ denote the perturbed eigenvectors and eigenvalues. To analyze the perturbation effect in detail, we resort to the small perturbation assumption [13]. Small perturbation theory on matrices [16], [17] and graphs [18], [19], [20], found different applications, such as spectral clustering [20][18] or Laplacian eigenvector localization [19]. In [13], topology uncertainties with implications for clustering and semi-supervised learning are analyzed, with results relevant to time-varying signal on graphs processing [21] and graph learning [22].

In [13], a small perturbation analysis is carried out, whose main results we recall here. Specifically, it is shown that the eigenvalues of the perturbed Laplacian $\tilde{\mathbf{L}}$ are approximated as

$$\tilde{\lambda}_i \approx \lambda_i + \sum_{m\in\mathcal{E}_p} C_m^{(i)}\sigma_m \tag{4}$$

where $\mathcal{E}_p$ is the set of perturbed edges and

$$C_m^{(i)} = [\mathbf{u}_i(m_1) - \mathbf{u}_i(m_2)]^2$$

is the square of the (discrete) gradient of the eigenvector $\mathbf{u}_i$ along the edge $m$, that is the edge connecting the nodes $m_1$, $m_2$. The notation $\mathbf{u}_i(m_1)$ corresponds to the $m_1$-th entry of $\mathbf{u}_i$ eigenvector.

Similarly, the eigenvectors of the perturbed Laplacian $\tilde{\mathbf{L}}$ are approximated as

$$\tilde{\mathbf{u}}_i \approx \mathbf{u}_i + \sum_{m\in\mathcal{E}_p} \mathbf{u}_j \sum_j B_m^{(i,j)}\sigma_m \tag{5}$$

where

$$B_m^{(i,j)} = \frac{\Delta_m^{(i)}\Delta_m^{(j)}}{\lambda_i - \lambda_j}$$

where $\Delta_m^{(i)} = \mathbf{u}_i(m_1) - \mathbf{u}_i(m_2)$ is the variation of the eigenvector values at the nodes $m_1$, $m_2$ of the $m$-th edge, namely across the $m$-th edge.

In the following section, we show how to merge multiple graphs by applying weights based on prior knowledge from probabilistic modeling and graph perturbation analysis.

## III. Robust Clustering

In this section, we derive a method to combine multiple graphs obtained from different measurements to make spectral clustering more stable with respect to random fluctuations of the measurements. To illustrate the method, we derive first a statistical analysis of the eigenvalues/eigenvectors perturbations resulting from graph inferences affected by errors. Then, we propose a method to optimally combine the eigenvectors in order to minimize the variance of the estimate and thus achieve a robust spectral clustering.

We start with the statistical model of perturbations affecting a single graph. Then, we will extend this analysis to multiple graphs, deriving the optimal combination of multiple measurements, which will then be applied in the next section to real-world problems in brain network inference.

### A. Single-Graph Estimate

The availability of a prior $P_m$, $m=1,\cdots M$, with $M = N \times N$, on the perturbation representing the graph observation error enables us to compute the expected values and variances of the perturbed eigenvalues $\lambda_i$ and eigenvectors $\mathbf{u}_i$, $i = 1,\cdots N$. Briefly, our analysis utilizes the approach presented in [13], where the effect of small perturbations is approximated as a linear superposition of perturbation components. Given the prior

$P_m$ for each perturbation event, $m=1,\cdots M$, represented by the binary random variable $z_m$, the expected values and variances can be directly calculated. Herein, we summarize the main results.

We start with the following approximation of the perturbed eigenvalue

$$\tilde{\lambda}_i = \lambda_i + \sum_m C_m^{(i)} \sigma_m \; z_m \tag{6}$$

where $z_m, m=1,\cdots M$, are a set of random variables defined in (1). The expected value of $\tilde{\lambda}_i$ with respect to the random variable $z_m$, $m=1,\cdots M$ is then

$$\begin{aligned} E\{\tilde{\lambda}_i\} &= \lambda_i + \sum_m C_m^{(i)} \sigma_m \; E\{z_m\} \\ &= \lambda_i + \sum_m C_m^{(i)} \sigma_m \; P_m \end{aligned} \tag{7}$$

and its variance is given by

$$\begin{aligned} \mathrm{Var}\{\tilde{\lambda}_i\} &= \sum_m \left(C_m^{(i)}\right)^2 \; \mathrm{Var}\{z_m\} \\ &= \sum_m \left(C_m^{(i)}\right)^2 \; (1-P_m) \; P_m. \end{aligned} \tag{8}$$

Similarly, for the $i$-th perturbed eigenvector, we have:

$$\tilde{\mathbf{u}}_i = \mathbf{u}_i + \sum_{j,j\neq i} \mathbf{u}_j \sum_m B_m^{(i,j)} \sigma_m \; z_m, \tag{9}$$

and then

$$E\{\tilde{\mathbf{u}}_i\} = \mathbf{u}_i + \sum_{j,j\neq i} \mathbf{u}_j \sum_m B_m^{(i,j)} \sigma_m \; P_m \tag{10}$$

and

$$\begin{aligned} \mathrm{Cov}\{\tilde{\mathbf{u}}_i, \tilde{\mathbf{u}}_i\} = &\sum_{j_1,j_1\neq i} \sum_{j_2,j_2\neq i} \mathbf{u}_{j_1} \mathbf{u}_{j_2}^T \\ &\cdot \sum_m B_m^{(i,j_1)} B_m^{(i,j_2)} \; (1-P_m) \; P_m. \end{aligned} \tag{11}$$

Finally, note that the perturbed eigenvalues and eigenvectors are correlated. For example, the covariance of two perturbed eigenvectors is:

$$\begin{aligned} \mathrm{Cov}\{\tilde{\mathbf{u}}_{i_1}, \tilde{\mathbf{u}}_{i_2}\} = &\sum_{j_1,j_1\neq i_1} \sum_{j_2,j_2\neq i_2} \mathbf{u}_{j_1} \mathbf{u}_{j_2}^T \\ &\cdot \sum_m B_m^{(i_1,j_1)} B_m^{(i_2,j_2)} \; (1-P_m) \; P_m. \end{aligned} \tag{12}$$

This covariance could, in principle, be used to enhance eigenvector estimation. However, given the limitations of small perturbation assumptions in brain network analysis, the improvement expected from incorporating perturbed eigenvector covariance in eigenvector estimation is likely limited and will not be utilized in the following EEG data analysis.

Let us now specify the above results for the case of a data-driven prior $P_m$, $m=1,\cdots M$. We adopt the model in (3), separately considering the case of an absent edge ($w_m \leq \theta$), where an error corresponds to its addition ($\sigma_m = 1$), and, conversely, the case of a present edge ($w_m > \theta$), where a topology error leads to its removal ($\sigma_m = -1$).

Using the formulation in (3), the equations are rewritten as follows:

$$\begin{aligned} E\{\tilde{\lambda}_i\} &= \lambda_i + \sum_{m \; s.t. w_m \leq \theta} C_m^{(i)} \sigma_m \; w_m \\ &\quad + \sum_{m \; s.t. w_m > \theta} C_m^{(i)} \sigma_m \; (1-w_m) \\ &= \lambda_i + \sum_{m \; s.t. w_m \leq \theta} C_m^{(i)} w_m \\ &\quad + \sum_{m \; s.t. w_m > \theta} C_m^{(i)} (w_m - 1) \end{aligned} \tag{13}$$

$$\begin{aligned} E\{\tilde{\mathbf{u}}_i\} &= \mathbf{u}_i + \sum_j \mathbf{u}_j \sum_{m \; s.t. w_m \leq \theta} B_m^{(i,j)} \sigma_m \; w_m \\ &\quad + \sum_j \mathbf{u}_j \sum_{m \; s.t. w_m > \theta} B_m^{(i,j)} \sigma_m \; (1-w_m) \\ &= \mathbf{u}_i + \sum_j \mathbf{u}_j \sum_{m \; s.t. w_m \leq \theta} B_m^{(i,j)} \; w_m \\ &\quad + \sum_j \mathbf{u}_j \sum_{m \; s.t. w_m > \theta} B_m^{(i,j)} (w_m - 1) \end{aligned} \tag{14}$$

$$\begin{aligned} \mathrm{Cov}\{\tilde{\mathbf{u}}_i, \tilde{\mathbf{u}}_i\} = &\sum_{j_1,j_1\neq i} \sum_{j_2,j_2\neq i} \mathbf{u}_{j_1} \mathbf{u}_{j_2}^T \\ &\cdot \sum_m B_m^{(i,j_1)} B_m^{(i,j_2)} \; (1-w_m) \; w_m \end{aligned} \tag{15}$$

$$\begin{aligned} \mathrm{Cov}\{\tilde{\mathbf{u}}_{i_1}, \tilde{\mathbf{u}}_{i_2}\} = &\sum_{j_1,j_1\neq i_1} \sum_{j_2,j_2\neq i_2} \mathbf{u}_{j_1} \mathbf{u}_{j_2}^T \\ &\cdot \sum_m B_m^{(i_1,j_1)} B_m^{(i_2,j_2)} \; (1-w_m) \; w_m \end{aligned} \tag{16}$$

As a running example, we draw different samples of a Stochastic Block Model, specifically the Planted Partition Model (PPM), where an underlying node community partition is given [23]. In order to generate the nominal graph, we draw each random edge weight $w_m \in [0,1]$ from a conditional distribution determined by the probabilities $\mathbb{P}_s$ and $\mathbb{P}_d$, i.e., the probabilities of connecting nodes within the same community or across different communities. The weight $w_m$ of the $m$-th edge is matched against a threshold $\theta = 0.5$ as in (2) to derive a binary adjacency matrix $\mathbf{A}$. To simulate uncertainty, we introduce perturbations on $\mathbf{A}$ by randomly flipping edges from 1 to 0 or viceversa, according to the probability $P_m$ as in (3). This process generates a binary perturbed graph that will be used in the following analyses. For each nominal graph, we generate 5000 perturbed versions, and repeat the process across 50 independently original graphs.

Fig. 3 aims to validate the data generation model by showing the sample means of eigenvalues with their expected values and standard deviations. For $\lambda_2$ (in red) and $\lambda_6$ (in blue), we show sample means obtained by averaging over 50 graphs and 5000 iterations (dotted lines), as well as their expected values averaged over 50 graphs, including standard deviations. In this simulation,

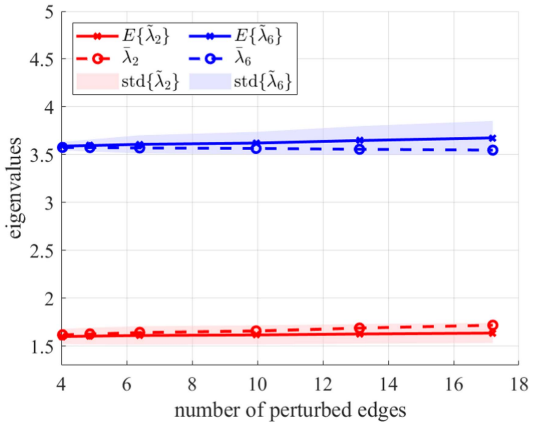


Fig. 3. Representation of sample mean of eigenvalues and their expected values with standard deviations. For the $\lambda_2$ (in red) and $\lambda_6$ (in blue) we represent their sample mean obtained averaging on 50 graphs and 5000 iterations (dot lines) and their expected values averaged over 50 graphs together with their stardard deviations. For this simulation $\mathbb{P}_s = 0.95$.

$\mathbb{P}_s = 0.95$. These results indicate that the sample means are close to the expected value, as it falls within the interval of $\pm$ std$\{\tilde{\lambda}_i\}$, and it means that the generated graphs follow the small perturbation model.

### B. Combinations of Multiple Observations

When multiple clinical trials or subjects are available, it is of interest to find out how to combine the multiple graphs resulting from different operating conditions to find a possibly common structure. Relying on spectral clustering, it is useful to find a common set of eigenvalues and eigenvectors to be used for clustering. In principle, we could either 1) build a weighted Laplacian matrix, combining the Laplacians pertaining to the different graphs, and then use the eigen-decomposition of this weighted Laplacian, or 2) take a linear weighted combination of the eigenvalues and take a similar weighted combination of the eigenvectors. In the following, we will adopt this second approach and find the optimal weights, based on the statistical analysis carried out in the previous section. Then, we will compare the performance of the two methods to determine the best strategy.

Let us suppose that $K$ independent observations of the graph are available, resulting in a set of observed eigenvalue and eigenvectors $\tilde{\lambda}_i^{(k)}$, $\tilde{\mathbf{u}}_i^{(k)}$, for $i=1,\cdots N$, $k=1,\cdots K$, where $i$ indicates the order of the eigenvalue, while $k$ indicates the graph. The $m$-th edge on each graph is subject to independent perturbations with probability $P_m^{(k)}$, $k=1,\cdots K$.

We take a convex linear combination of the eigenvalues pertaining to the different graphs using $K$ weights $\alpha_i^{(k)}$, $k=0,\cdots K-1$, with $\alpha_i^{(k)} \geq 0$ and $\sum_{k=0}^{K-1} \alpha_i^{(k)} = 1$. The resulting eigenvalues are then:[1]

$$\hat{\lambda}_i = \sum_k \alpha_i^{(k)} \tilde{\lambda}_i^{(k)}$$

$$= \sum_k \alpha_i^{(k)} \left( \lambda_i + \sum_m C_m^{(i)} \sigma_m^{(k)} \; z_m^{(k)} \right)$$

$$= \lambda_i + \sum_m C_m^{(i)} \sum_k \alpha_i^{(k)} \sigma_m^{(k)} \; z_m^{(k)}; \tag{17}$$

Later on, we will provide an algorithm to optimize the choice of the weights $\alpha_i^{(k)}$. Before doing that, we anticipate that, once obtained the optimal weights, we will use them to weight also the eigenvectors associated to different graphs to obtain a new set of vectors that will be then used to find the clusters. The weighted combination of the eigenvectors can be expressed as:[2]

$$\hat{\mathbf{u}}_i = \sum_k \alpha_i^{(k)} \tilde{\mathbf{u}}_i^{(k)}$$

$$= \sum_k \alpha_i^{(k)} \left( \mathbf{u}_i + \sum_{j, j \neq i} \mathbf{u}_j \sum_m B_m^{(i,j)} \sigma_m^{(k)} \; z_m^{(k)} \right)$$

$$= \mathbf{u}_i + \sum_{j, j \neq i} \mathbf{u}_j \sum_m B_m^{(i,j)} \sum_k \alpha_i^{(k)} \sigma_m^{(k)} \; z_m^{(k)} \tag{18}$$

To find the optimal weights, we leverage on the statistical properties (mean and variance) of the eigenvalues. In particular, the expected value of the $i$-th eigenvalue is:

$$E\{\hat{\lambda}_i\} = \lambda_i + \sum_m C_m^{(i)} \sum_k \alpha_i^{(k)} \sigma_m^{(k)} \; E\{z_m^{(k)}\}$$

$$= \lambda_i + \sum_m C_m^{(i)} \sum_k \alpha_i^{(k)} \sigma_m^{(k)} \; P_m^{(k)} \tag{19}$$

while the variance is:

$$\mathrm{Var}\{\hat{\lambda}_i\} = \sum_k \sum_m \left( C_m^{(i)} \right)^2 \; \left( \alpha_i^{(k)} \right)^2 \; \mathrm{Var}\{z_m^{(k)}\}$$

$$= \sum_k \sum_m \left( C_m^{(i)} \right)^2 \; \left( \alpha_i^{(k)} \right)^2 \; (1 - P_m^{(k)}) \; P_m^{(k)}$$

$$= \boldsymbol{\alpha}_i^T \Gamma_i \boldsymbol{\alpha}_i \tag{20}$$

where $\boldsymbol{\alpha}_i$ is a column vector whose generic element $\alpha_i^{(k)}$ is the weight associated to the $i-$th eigenvalue of the $k-$th estimate and $\Gamma_i$ is a $K \times K$, positive semidefinite diagonal matrix whose $k$-th diagonal element is $\sum_m (C_m^{(i)})^2 \; (1 - P_m^{(k)}) \; P_m^{(k)}$, which corresponds to $\sum_m (C_m^{(i)})^2 \; (1 - w_m^{(k)}) \; w_m^{(k)}$ according to our model.

Now, we propose a method to compute the optimal weights $\alpha_i^{(k)}$ in order to minimize the variance in (20). More specifically, we propose to find the optimal weights as the solution of the following optimization problem, that corresponds to the minimization of the variance associated to each eigenvalue at

[1] It is useful to point out that the values $\hat{\lambda}_i$ obtained in this way are not proper eigenvalues of any matrix; we keep calling them weighted eigenvalues only to remind that their values come from a weighted combination of eigenvalues.

[2] Let us notice that also in this case, as with the eigenvalues, the weighted combinations of eigenvectors does not lead to proper eigenvectors of any matrix. We keep calling them weighted eigenvectors because we use them in a similar way to what is done in spectral clustering to find the clusters.

the different layers:

$$\begin{aligned} \boldsymbol{\alpha_i} &= \arg\min_{\boldsymbol{\alpha}\in\mathbb{R}^K} \mathrm{Var}\{\hat{\lambda}_i\} = \arg\min_{\boldsymbol{\alpha}\in\mathbb{R}^K} \boldsymbol{\alpha}^T \Gamma_i \boldsymbol{\alpha} \\ \text{s.t.} \quad & \boldsymbol{\alpha}_i^T \cdot \mathbf{1} = 1 \\ & \boldsymbol{\alpha}_i \geq \mathbf{0} \end{aligned} \tag{21}$$

By applying the Karush-Kuhn-Tucker conditions [24] to the above problem, we obtain the following closed-form solution:

$$\alpha_i^{(k)} = \frac{\left[\sum_m \left(C_m^{(i)}\right)^2 P_m^{(k)}(1-P_m^{(k)})\right]^{-1}}{\sum_k \left[\sum_m \left(C_m^{(i)}\right)^2 P_m^{(k)}(1-P_m^{(k)})\right]^{-1}} \tag{22}$$

The previous formula balances the effects of perturbations on the $m$-th edge of the $k$-th observation by incorporating the reliability of the edge estimate, represented by $P_m^{(k)}(1-P_m^{(k)})$, and the potential impact of the error on the $i$-th eigenvalue estimation, reflected in the factor $C_m^{(i)}$. Thus, the weights $\boldsymbol{\alpha}_i$ that minimize the variance of the $i$-th eigenvalue estimate serve as a practical measure of the reliability of the estimation for the $i$-th eigenvector subspace component.

Building on this argument, we use the same weights also for the combination of the eigenvectors, as they indicate the importance of each spectral component, as in (18). In this way, we can derive the probabilistic characterization of the weighted eigenvectors as follows:

$$E\{\hat{\mathbf{u}}_i\} = \mathbf{u}_i + \sum_{j,j\neq i} \mathbf{u}_j \sum_m B_m^{(i,j)} \sum_k \alpha_i^{(k)} \sigma_m^{(k)} \; P_m^{(k)} \tag{23}$$

and

$$\begin{aligned} \mathrm{Cov}\{\hat{\mathbf{u}}_i\} = & \sum_{j_1,j_1\neq i} \sum_{j_2,j_2\neq i} \mathbf{u}_{j_1} \mathbf{u}_{j_2}^T \\ & \cdot \sum_m B_m^{(i_1,j_1)} B_m^{(i_2,j_2)} \sum_k \left(\alpha_i^{(k)}\right)^2 (1-P_m^{(k)}) \; P_m^{(k)} \end{aligned} \tag{24}$$

Before proceeding with the numerical test of our algorithm, it is worth to point out that, when taking the linear combination of the eigenvalues of order $i$ over all graphs, in principle there is no guarantee that the ordering of the weighted eigenvalues will respect the same ordering of the original eigenvalues. Here we provide a sufficient condition that the ordering is preserved. We can easily prove, in fact, that, if

$$\max_k \lambda_i^{(k)} < \min_k \lambda_{i+1}^{(k)}, \tag{25}$$

then the ordering between the eigenvalues of order $i$ and $i+1$ is preserved. The proof is quite simple, as it relies on the fact that the linear combination is a convex combination. This implies that

$$\min_k \lambda_i^{(k)} \leq \sum_k \alpha_i^{(k)} \tilde{\lambda}_i^{(k)} \leq \max_k \lambda_i^{(k)}.$$

As a consequence, if (25) holds, then we have:

$$\sum_k \alpha_i^{(k)} \tilde{\lambda}_i^{(k)} \leq \max_k \lambda_i^{(k)} < \min_k \lambda_{i+1}^{(k)} \leq \sum_k \alpha_{i+1}^{(k)} \tilde{\lambda}_{i+1}^{(k)}. \tag{26}$$

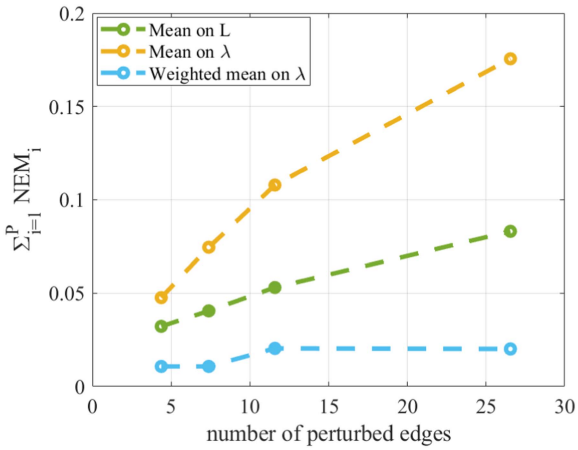


Fig. 4. Normalized Eigenvalue Mismatch for the sum of the first $P$ eigenvalues (excluding the first eigenvalue). For this simulation $\mathbb{P}_s = 0.95$, $N = 100$ and $P = 5$. Results are averaged on 50 graphs and 500 iterations.

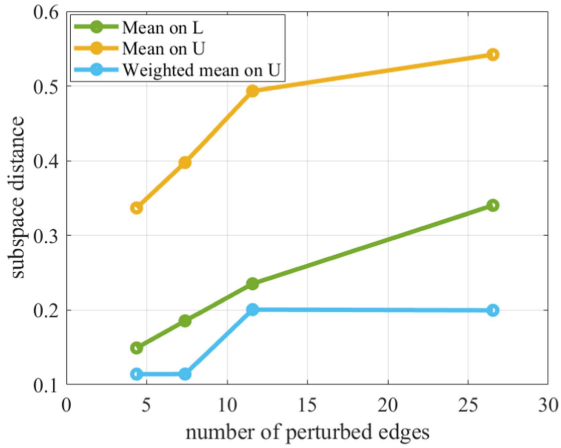


Fig. 5. Subspace distance vs number of perturbed edges. For this simulation $\mathbb{P}_s = 0.95$, $N = 100$ and $P = 5$. Results are averaged on 50 graphs and 500 iterations.

Now we test our method over PPM graphs in the case of multiple independent observations. Specifically, we consider $K = 3$, $\mathbb{P}_S = 0.95$, $N = 100$ and a number of community $P = 5$. The results presented are averages across 50 graphs and 500 iterations. In Fig. 4 we show the Normalized Eigenvector Mismatch (NEM), that is computed as $|\lambda_i - \hat{\lambda}_i|/\lambda_i$, as the number of perturbed edges varies. The light blue curve represents eigenvalues obtained with optimal weighting, the orange curve represents eigenvalues obtained by directly averaging the eigenvalues of the $K$ estimates, and the green curve represents eigenvalues obtained by performing the eigen-decomposition of the sample mean of the graph Laplacians of the $K$ estimates.

Fig. 5 shows the Grassmann subspace distance [25] between the estimated subspace and the ground truth under three conditions: optimal weighted mean of Laplacian eigenvectors from each of the $K$ estimates (light blue), mean on the original eigenvectors (orange), and eigenvectors obtained from the eigen-decomposition of the sample mean of the $K$ graph Laplacians (green). We remark that the Grassmann distance [25] between

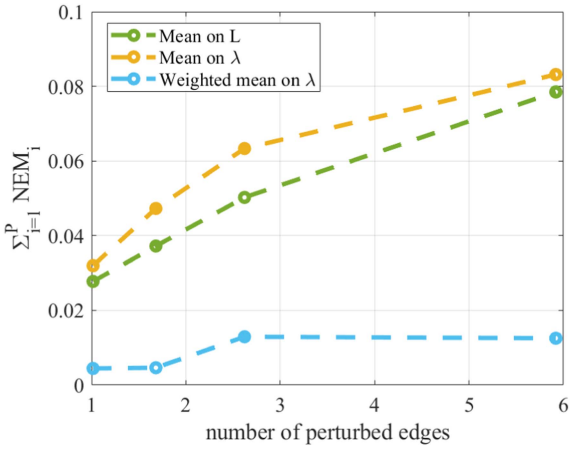


Fig. 6. Normalized Eigenvalue Mismatch for the sum of the first $P$ eigenvalues (excluding the first eigenvalue). For this simulation $\mathbb{P}_s = 0.95$, $N = 50$ and $P = 4$. Results are averaged on 50 graphs and 500 iterations.

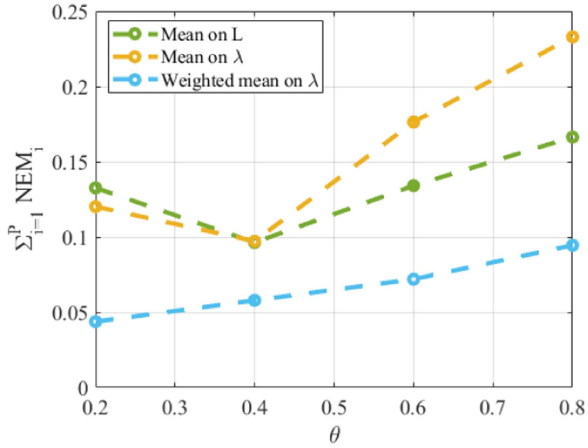


Fig. 8. Normalized Eigenvalue Mismatch as a function of the threshold $\theta$. For this simulation $\mathbb{P}_s = 0.95$, $N = 50$ and $P = 4$. Results are averaged on 50 graphs and 500 iterations.

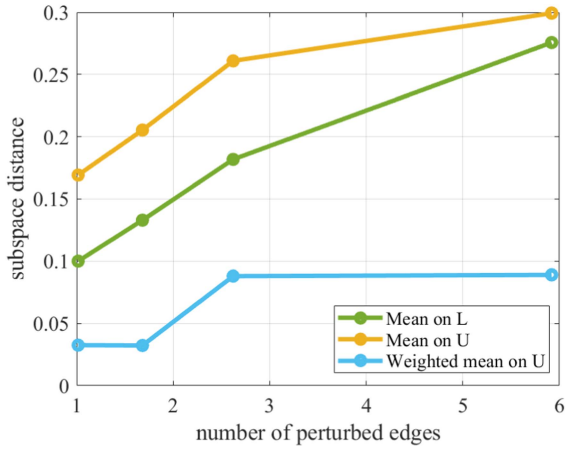


Fig. 7. Subspace distance vs number of perturbed edges. For this simulation $\mathbb{P}_s = 0.95$, $N = 50$ and $P = 4$. Results are averaged on 50 graphs and 500 iterations.

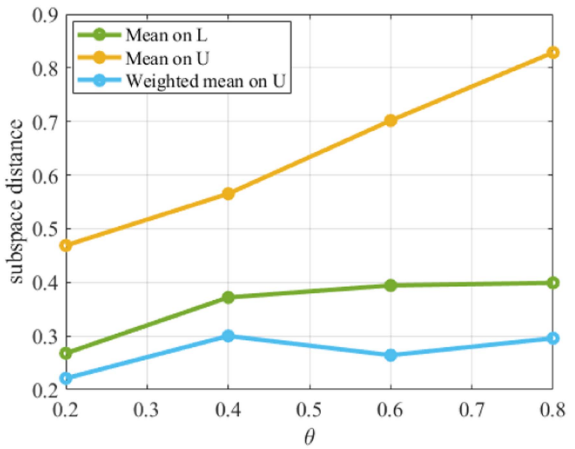


Fig. 9. Grassmann subspace distance as a function of the threshold $\theta$. For this simulation $\mathbb{P}_s = 0.95$, $N = 50$ and $P = 4$. Results are averaged on 50 graphs and 500 iterations.

two subspaces is expressed by the principal angles, derived through the singular value decomposition (SVD) of the product of their orthonormal bases.

Figs. 6 and 7 present similar results, but for a network of $N = 50$ nodes composed by $P = 4$ communities.

From all these figures, we can observe that the method of optimally combining the eigenvectors of each graph outperforms all other methods. In both synthetic scenarios, we can observe that the subspace distance between the optimal weighted eigenvectors and the ground truth is lower compared to the two alternatives. The advantage of using weighted eigenvectors is especially evident as the number of perturbed edges increases.

An important parameter in our study is the threshold value $\theta$, which determines the binarization of the weighted original graph and, consequently, the final network topology. To evaluate the robustness of our method in function of $\theta$, we focus on analyzing the effect of this parameter while isolating its influence from other factors by keeping the number of perturbed edges approximately fixed at 10. We consider the same scenario of the previous experiments and we vary the threshold $\theta$ in the range $[0.2, 0.8]$. In Fig. 8, we report the NEM, while Fig. 9 shows the Grassmann subspace distance between perturbed and ground truth scenarios. In both cases, our proposed method (light blue curve), outperforms the baseline strategies, namely the mean on the Laplacians (green) and the mean on eigenvalue/eigenvectors (orange). This result highlights that, across a wide range of $\theta$ values, our method remains robust and more accurate in recovering both the spectral content and the eigenspace structure.

The code to perform these analysis in synthetic scenarios is available at [26].

## IV. Application to Brain Functional Connectivity

In this section we apply the proposed robust graph inference model to real EEG data, by focusing on the development of the statistical model, spectral analysis and functional connectivity

estimation. Specifically, we use EEG signals from multiple public datasets acquired under various cognitive states. We showcase the potential of our approach to characterize brain reorganization processes when multiple graph estimates are obtained and integrated using small perturbation priors.

### A. Multiple Functional Connectivity Estimates as a Perturbation Prior

In this subsection, we detail how to identify and manage multiple functional connectivity estimates by integrating them to obtain an optimal graph topology.

In real EEG networks, multiple graph estimates of brain functional connectivity can be computed [6], [27]. Here, we consider each estimate as a noisy (perturbed) approximation of a nominal graph underlying the observations, representing the ground truth brain connectivity.

EEG-based brain network analysis utilizes various estimators, such as spectral coherence [28], imaginary coherence [29], and phase difference [12], selected based on the specific task and experimental design [6]. Depending on the chosen estimator, functional connectivity can be defined within frequency bins or bands, or it may inherently integrate multiple trials.

In this context, multiple graph estimates may arise from the use of different connectivity estimators, the application of the same estimator across various frequency bands, or even from repeated trials or different subjects [3], [7], [30]. Each graph estimate is modeled as a perturbed version of a nominal graph, with perturbations that results from noise, variability in estimators, or differences across trials or subjects. It is important to remark that, in real EEG applications, the ground truth brain network is unknown. For reference purposes, we adopt the average across multiple observations as a ground truth.

Let us consider the EEG time series $s_n[t], t = 0, \dots, T-1$, at electrodes $n = 1, \cdots N$, and $\mathcal{P}_n(\omega_l) = M_n(\omega_l) \cdot \exp(j\varphi_n(\omega_l))$, $\omega_l = 2\pi l/T$, are the samples of the power spectral density at the $n$-th electrode. Besides, let

$$\mathcal{P}^{(nor)}_{m_1m_2}(\omega_l) = \mathcal{P}_{m_1m_2}(\omega_l)/\sqrt{\mathcal{P}_{m_1}(\omega_l)\mathcal{P}_{m_2}(\omega_l)}$$

for $m_1, m_2 = 1, \cdots N$ denote the normalized power cross-spectral density between the $m_1$-th and $m_2$-th electrodes at frequency $\omega_l$, $l = 0, \dots, T-1$, respectively. We now formally introduce here the functional connectivity measures employed in this work, which are the spectral coherence $C_{m_1m_2}$ [28], imaginary coherence $IC_{m_1m_2}$ [29], and phase difference $PD_{m_1m_2}$ [12]. These connectivity estimators are defined as follows:

$$C^{(B)}_{m_1m_2} = \frac{1}{||B||} \sum_{\omega_l=0}^{||B||-1} \left|\mathcal{P}^{(nor)}_{m_1m_2}(\omega_l)\right| \tag{27}$$

$$IC^{(B)}_{m_1m_2} = \frac{1}{||B||} \sum_{\omega_l=0}^{||B||-1} \left|\text{Im}\{\mathcal{P}^{(nor)}_{m_1m_2}(\omega_l)\}\right| \tag{28}$$

$$PD^{(B)}_{m_1m_2} = \frac{1}{||B||} \sum_{\omega_l=0}^{||B||-1} \left|\varphi_{i_1}(\omega_l) - \varphi_{i_2}(\omega_l)\right| \tag{29}$$

where the $B$ denotes the frequency band of interest and $||B||$ its cardinality. The presented estimators differ in both meaning and range: a functional connection between the $m_1$-th and $m_2$-th nodes corresponds to a large value of coherence and to small values of imaginary coherence and phase difference. To align these measures, we consider the transformed versions, normalized within $[0, 1]$:

$$\begin{aligned}
\mathcal{C}^{(B)}_{m_1m_2} &= \frac{C^{(B)}_{m_1m_2}}{\max\limits_{m_1,m_2} C^{(B)}_{m_1m_2}} \\
\mathcal{IC}^{(B)}_{m_1m_2} &= 1 - \frac{IC^{(B)}_{m_1m_2}}{\max\limits_{m_1,m_2} IC^{(B)}_{m_1m_2}} \\
\mathcal{PD}^{(B)}_{m_1m_2} &= 1 - \frac{PD^{(B)}_{m_1m_2}}{\max\limits_{m_1,m_2} PD^{(B)}_{m_1m_2}}
\end{aligned} \tag{30}$$

Fig. 10(a), (b) and (c) show the EEG-based functional connectivity estimators $\mathcal{C}^{(B_\beta)}_{m_1m_2}$, $\mathcal{IC}^{(B_\beta)}_{m_1m_2}$, and $\mathcal{PD}^{(B_\beta)}_{m_1m_2}$, for one subject from the BCI competition IV dataset 1 [31], in the beta band $B_\beta$, corresponding to $14-29$ Hz; for better visibility, only the 30 strongest weighted edges are shown.

We collect the normalized connectivity estimates over all the node pairs $(m_1, m_2)$, $m_1, m_2 = 1, \cdots N$, into three real weight adjacency matrices, denoted as $A^{(B)}_{\mathcal{C}}$, $A^{(B)}_{\mathcal{IC}}$, $A^{(B)}_{\mathcal{P}}$. The matrices are estimates of the functional connectivity graphs, and can be dealt by the previously described probabilistic approach. With these positions, it is safely assumed that near zero values $A^{(B)}_{\mathcal{C}}$, $A^{(B)}_{\mathcal{IC}}$ and $A^{(B)}_{\mathcal{PD}}$ intuitively occur in absence of a significant correlation between the edge nodes activity; similarly, values of $A^{(B)}_{\mathcal{C}}$, $A^{(B)}_{\mathcal{IC}}$ and $A^{(B)}_{\mathcal{PD}}$ are close to one in presence of correlated activity at the graph node. For intermediate values, the discrimination of the presence of a link from functional connectivity estimates between the EEG signal recorded at scalp electrodes becomes less reliable and more prone to perturbation errors.

Therefore, we rely on (3) to infer the probability of edge miss-classification. Specifically, we binarize each estimated adjacency matrix by thresholding against a threshold $\theta$, selected to maintain a fixed percentage of links. Then, we associate a probability of perturbation to each node pair $(m_1, m_2)$ so as to match the reliability of the thresholding result. Specifically, if a binary link is detected, the perturbation probability $P_m$ represents a false alarm probability, increasing with the weight distance from 1; hence, we use $P_m = 1 - w_m$. Conversely, if a binary link is not detected, the probability $P_m$ represents a false alarm, increasing with the weight distance from 0, and it is set as $P_m = w_m$. With these positions, each node pair $(m_1, m_2)$ is assigned a probability of edge misclassification.

Although the edges are supposedly prone to an error event, their impact on the graph spectral analysis depend on the graph topology. In the following we will show how to exploit the perturbation priors to identify the most critical edge for functional connectivity characterization.

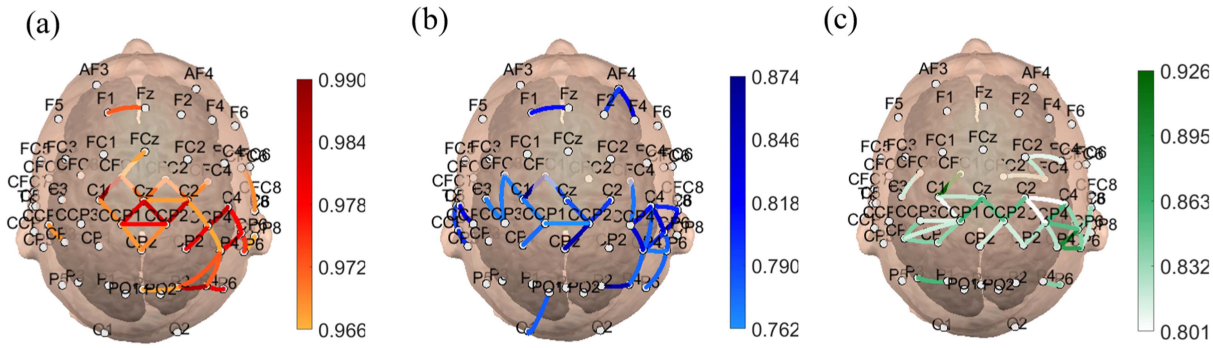


Fig. 10. Representation of the normalized functional connectivity estimators for the 30 strongest weighted edges in the $B_\beta$ band for a single subject. In panel a) we have coherence $\mathcal{C}_{m_1m_2}^{(B_\beta)}$, in b) imaginary coherence $\mathcal{IC}_{m_1m_2}^{(B_\beta)}$ and in c) phase difference $\mathcal{PD}_{m_1m_2}^{(B_\beta)}$. Collecting the estimator values over all the node pairs $(m_1, m_2)$ yields three real weight adjacency matrices $A_{\mathcal{C}}^{(B_\beta)}$, $A_{\mathcal{IC}}^{(B_\beta)}$, and $A_{\mathcal{P}}^{(B_\beta)}$.

### B. Spectral Analysis With Perturbation Priors

In this subsection, we explore the robustness of eigenvalues and eigenvectors of Laplacian matrix obtained from brain networks under the proposed statistical model. Specifically, we show how the theoretical results derived in previous sections can be directly used to identify critical nodes and edges in practical scenarios, such as functional EEG networks. In neuroscience applications, assessing the reliability of single graph estimates is fundamental to interpret brain connectivity. Here, we consider the simplified scenario of single graph, without multiple observations, to identify the most critical graph elements and highlight the interpretability of perturbation effects.

Small changes in the graph topology—such as those caused by uncertainties in functional connectivity estimate can lead to deviations in the spectral properties of the graph. By analyzing those deviations, we can understand how sensitive certain network components (nodes and edges) are to perturbations.

It is possible to write the error probability for the $i$-th eigenvalue that its estimated value differ from its nominal value more than a given threshold $\vartheta$ as:

$$\pi_{\lambda_i}(\vartheta) = \Pr\left\{\tilde{\lambda}_i - \lambda_i > \vartheta\right\} \tag{31}$$

This quantity is upper bounded based on the error range based on the Hoeffding's bound [32]:

$$\pi_{\lambda_i}(\vartheta) \leq \exp\left(-\frac{(\vartheta - (E\{\tilde{\lambda}_i\} - \lambda_i))^2}{2\sum_m \left(C_m^{(i)}\right)^2}\right) \tag{32}$$

where the bias term is:

$$E\{\tilde{\lambda}_i\} - \lambda_i = \sum_m C_m^{(i)} \sigma_m P_m$$

The formulation (32) allows us to quantify the robustness of the eigenvalues, that is expressed in terms of graph topology associated to the $m-$th edge. In Fig. 11 we report the $\sum_i C_m^{(i)}$ summed over the first $P$ components, i.e. $i = 1 \ldots P$, with $P$ the number of graph communities. This quantity is represented on the colors of graph edges in the figure, where only the 3% of most critical edges in terms of eigenvalue perturbations are represented for readability. Then, we consider the node degree of each node when the weight of each link correspond to the sum of $\sum_i C_m^{(i)}$ on the first P components to derive a way to measure how much each node is prone to eigenvalue perturbations. This is represented in the figure with the colors at graph nodes.

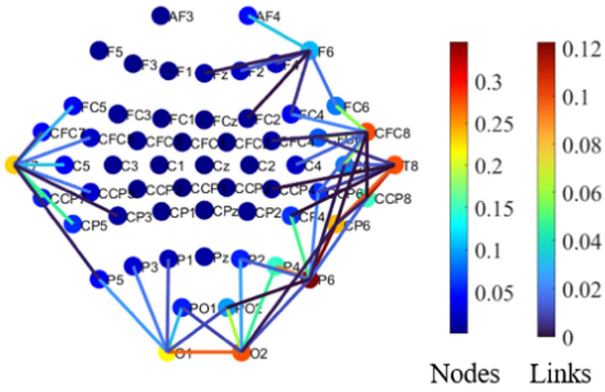


Fig. 11. Results of critical edges in terms of eigenvalue perturbation. We represent the 3% of most critical edges (colored according to Links colorbar) and nodes are represented according to the node degree computed weighting each link with its Hoeffding's bound (Nodes colorbar). EEG data are from BCI competition IV dataset during resting state.

In a similar way, we can derive the error probability for the the $i$-th eigenvector, considering the $n$-th coefficient,r to overcome a given threshold $\vartheta$:

$$\pi_{\mathbf{u}_i}(n;\vartheta) = \Pr\left\{\tilde{\mathbf{u}}_i[n] - \mathbf{u}_i[n] > \vartheta\right\} \tag{33}$$

This probability is upper bounded based on the error range based on the Hoeffding's bound [32] as:

$$\pi_{\mathbf{u}_i}(n;\vartheta) \leq \exp\left(-(\vartheta - (E\{\tilde{\mathbf{u}}_i[n]\} - \mathbf{u}_i[n]))^2)/2\sum_m \left(\delta u_m^{(i)}[n]\right)^2\right) \tag{34}$$

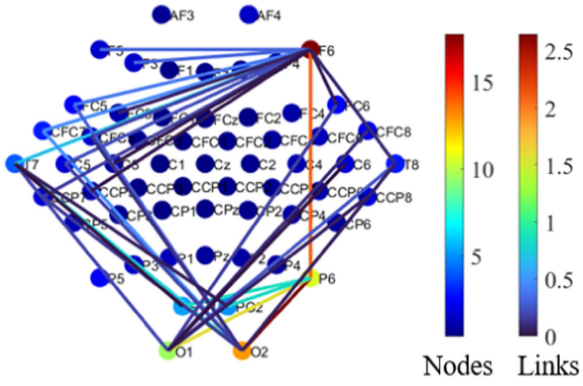


Fig. 12. Results of critical edges in terms of eigenvector perturbation. We represent the edges related to the perturbations of the $3^{rd}$ eigenvector. We represent the most critical edges (colored according to the Links colorbar) and nodes are represented according to the node degree computed weighting each link with its Hoeffding's bound (Nodes colorbar). EEG data are from BCI competition IV dataset during resting state.

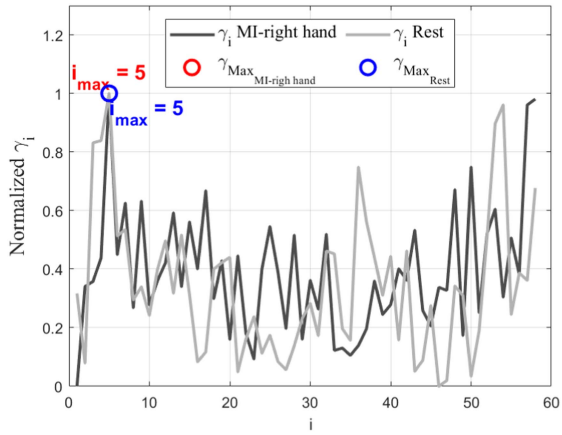


Fig. 13. Gap for real EEG data recorded during resting state for MI of right hand and rest subject for optimally combined eigenvalues. Curves in the figure are obtained under two conditions of MI (dark gray) and rest (light grey).

where the bias term is computed as

$$E\{\tilde{\mathbf{u}}_i[n]\} - \mathbf{u}_i[n] = \sum_m \sum_{j,j\neq i} \mathbf{u}_j[n] B_m^{(i,j)} \sigma_m P_m$$

and the $\delta u_m^{(i)}[n]$ term is as follows:

$$\delta u_m^{(i)}[n] = \sum_{j,j\neq i} \mathbf{u}_j[n] B_m^{(i,j)} = \Delta_m^{(i)} \sum_{j,j\neq i} \mathbf{u}_j[n] \frac{\Delta_m^{(j)}}{\lambda_i - \lambda_j}$$

In order to directly investigate the role of the different edges of the brain network in determining the eigenvector perturbation we consider the denominator in exponential argument of (34). We represent this quantity for the third eigenvector and we represent it as a signal on edges colored with the link colorbar. Then we consider its degree in order to have a measure for to illustrate which nodes of the networks are more prone to estimation errors.

In Fig. 11 we show the results using EEG data from BCI competition IV dataset during resting state. Based on the above analysis, we highlight the 3% most critical links in terms of eigenvalue perturbation, as indicated in the *Links* colorbar. We also highlight the critical nodes, by summing up the Hoeffding's bound of the links stemming from it, as indicated in the *Nodes* colorbar. Fig. 12 show analogous results provided by the perturbation analysis of the 3-rd eigenvector of the same graph. We decide to show the perturbation of the third eigenvector in Fig. 12 because, Laplacian eigenvectors associated with the smallest eigenvalues are more descriptive of the graph structure. Among these, we selected one for visualization purposes to provide a clear representation. Figs. 11 and 12 show that, both from an eigenvalue and an eigenvector perspective, the nodes that are topologically more prone to perturbation errors are the peripheral nodes in the brain networks. Interestingly, critical graph edges always contain a peripheral node, but while in the case of eigenvalue perturbation, they tend to be short-distance links, in the case of eigenvector perturbations, the critical edges are long-range connections that span from one extreme to the other of the graph. These measures of node and edge criticality can be leveraged for data preprocessing, potentially allowing the removal of the most critical components.

### C. Identification of the Number of Brain Communities

The study of brain functional connectivity organization is fundamental in characterizing human cognitive processes. Indeed, different brain states present connectivity interaction patterns between distinct regions [33]. These interactions form functional communities in the brain-groups of nodes (regions) that exhibit higher levels of connectivity with each other than with other regions. Identifying these communities is essential for understanding how different cognitive tasks, such as those in motor imagery experiments (where a brain response is triggered by imagining a motor task), or in disease states affect brain network organization [3], [34], [35].

In this subsection, we focus on how to determine the number of graph communities in two different applications, which correspond to motor imagery experiments, from BCI competition IV [14] and Alzheimer's disease, from [15].

With the aim to identify the number of communities $P$, we use eigenvalue gap with $P = \arg\max_i \gamma_i$, with $\gamma_i = \lambda_i - \lambda_{i-1}$, $i = 2, \cdots N.$, already used in EEG networks [36], [37]. The eigenvalue perturbation satisfies $\gamma_i \leq \lambda_i - \tilde{\lambda}_i \leq \gamma_{i+1}$. In the case of multiple graph observation with optimal weights, we consider $\hat{\gamma}_i = \hat{\lambda}_i - \hat{\lambda}_{i-1}$.

We firstly consider EEG data recorded during motor imagery experiments from BCI competition IV [14], where EEG signal are recorded from $N = 59$ electrodes. We consider one subject performing motor imagery task of the right hand and we extract $K = 3$ connectivity estimates $A_{\mathcal{C}}^{B_\alpha}$, $A_{\mathcal{IC}}^{B_\alpha}$ and $A_{\mathcal{PD}}^{B_\alpha}$, computed in $B_\alpha$ frequency band ($[8-13]$ Hz). We optimally combine the eigenvalues from the different estimates and we compute the $\hat{\gamma}_i$. Fig. 13 represents the gap for real EEG data recorded during motor imagery experiments under two conditions (motor imagery (MI) of the right hand, in dark) and resting state (in blue) and we represent in red and blue circles the number of identified community. While our result indicate that the number

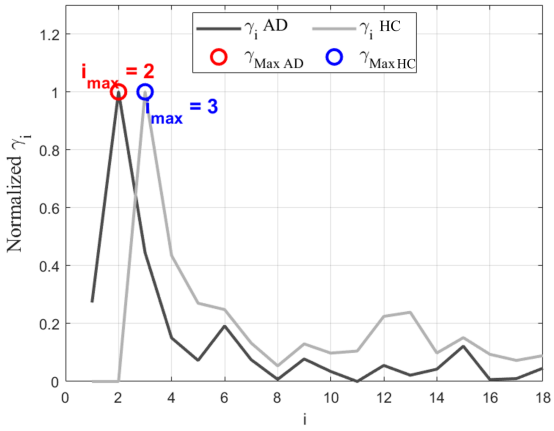


Fig. 14. Gap for real EEG data recorded during resting state for AD subject and healthy HC subject for optimally combined eigenvalues. Curves in the figure are obtained under two conditions of AD (dark gray) and HC (light grey).

of detected functional communities remains the same between the two mental states, the internal organization of these communities may differ across conditions, as we will show in the next subsection.

We aim to apply the eigenvalue gap approach to a different type of functional connectivity EEG network application, which is the characterization of human brain in Alzheimer's Disease (AD) [38]. To this end, we use EEG data from a public dataset [15] with EEG signals recorded from $N=19$ electrodes in a standard $10-20$ position [39]. In the context of AD, multilayer networks have been employed by considering several estimates in different frequency bands with a fixed functional connectivity measure [7]. For this reason, we consider the spectral coherence in $K=4$ frequency bands of interest, which are the $\theta$ bandwidth $B_\theta$, the $\alpha$ bandwidth $B_\alpha$, the $\beta$ bandwidth $B_\beta$, and the $\gamma$ bandwidth $B_\gamma$, corresponding to $4-7$Hz, $8-13$ Hz, $14-29$ Hz and $30-40$ Hz. With these positions, the adjacency matrices are $A_{\mathcal{C}}^{B_\theta}$, $A_{\mathcal{C}}^{B_\alpha}$, $A_{\mathcal{C}}^{B_\beta}$ and $A_{\mathcal{C}}^{B_\gamma}$. As described previously, we combine the eigenvalue estimates across different $K=1,\cdots 4$ to obtain the optimally weighted $\hat{\gamma}_i,\ i=1,\cdots N$ for two conditions: AD and Healthy Control (HC). Fig. 14 presents the results of our analysis of the optimally weighted gaps for EEG data recorded in AD and HC subjects. Our findings suggest that more connectivity structures ($i_{MAX}=3$) are present in control subjects compared to AD patients ($i_{MAX}=2$), indicating a less structured connectivity pattern in diseased states. This aligns with findings in Alzheimer-related literature that demonstrate a connectivity loss in AD [40].

One important parameter that impacts the analysis is the threshold used to binarize the functional connectivity matrices. This step determines which connections are retained and can impact the resulting network topology. In neuroscience applications, brain networks inferred from EEG, MEG, or fMRI data are usually represented as fully connected weighted graphs, where nodes correspond to brain regions and edges to their connectivity [27]. These graphs are often difficult to interpret and may include spurious connections from noise or artifacts [29]. To reduce complexity, thresholding techniques have been proposed

TABLE I
T-VALUES COMPUTED FROM A TWO-SAMPLE UNPAIRED T-TEST COMPARING THE POSITION OF $\gamma_{i_{\text{MAX}}}$ BETWEEN CONTROL AND AD GROUPS FOR DIFFERENT VALUES OF $\phi$

| $\phi$ (%) | 8 | 10 | 15 | 20 | 25 | 30 |
|---|---|---|---|---|---|---|
| t-values | 0.48 | 1.54 | 1.66 | 3.04 | 2.27 | 0.43 |

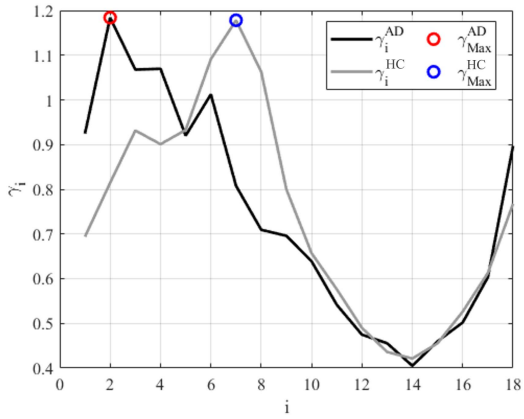


Fig. 15. Average eigenvalue gap $\gamma_i$ across subjects for AD (black line) and HC (gray line), for $\phi = 20\%$.

to filter meaningful links [41], including strategies based on connection strength, statistical testing, or indirect interaction correction [42]. Some approaches also use graph features, like preserving a fixed mean degree [43]. While threshold selection is important [44], it is not the core of our work [45]. We adopt a common method that retains the top $\phi$ percent of strongest links, allowing comparisons across different connectivity estimators.

To analyze the role of the threshold percentage parameter $\phi$, we consider AD related data with $A_{\mathcal{C}}^{B_\theta}$, $A_{\mathcal{C}}^{B_\alpha}$, $A_{\mathcal{C}}^{B_\beta}$ and $A_{\mathcal{C}}^{B_\gamma}$. For each subject, we compute the eigenvalue gaps $\hat{\gamma}_i$ from the optimally combined graph observations, and derive the position of the maximum gap ($i_{\text{MAX}}$) as an estimate of the number of communities. We perform a statistical analysis using unpaired t-test for different values of $\phi$. For each value of $\phi$, we compute the position of $\gamma_{i_{\text{MAX}}}$ across subjects in both groups (AD and HC) and used it as the test statistic. The results, reported in Table I, show that the t-value remains consistently positive across a broad range of $\phi$ values, reaching its maximum at $\phi = 20\%$. This indicates that the peak of the spectral gap tends to occur at lower indices in the AD subjects, suggesting a significant reduction of the number of communities compared to healthy subjects. This results, which is consistent with the hypothesis of connectivity loss in AD, is maintained over the considered values of $\phi$. For clarity, we also report in Fig. 15 the average eigenvalue gaps across all AD and HC subjects for $\phi = 20\%$, to show this separation in connectivity structure.

Further investigations on the connectivity reorganizations in AD patients will be found in Section E.

### D. Brain Community Detection

In this subsection, we use spectral clustering to detect communities in brain functional connectivity networks derived from

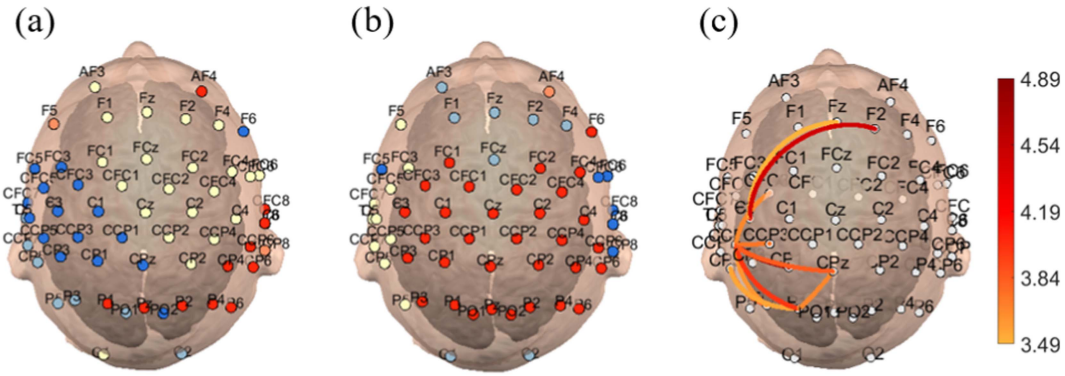


Fig. 16. Results of community detection on optimally weighted eigenvectors considering three network estimates: $A_{\mathcal{C}}^{B_\alpha}$, $A_{\mathcal{IC}}^{B_\alpha}$ and $A_{\mathcal{PD}}^{B_\alpha}$. In (a) we have communities found during motor imagery of the right hand, (b) during rest and in (c) we have results of the statistical t-test, highlighting the links that present a significant statistical difference between the motor imagery and rest conditions. All the results are obtained for $P = 5$.

EEG data. Specifically, we apply the eigenvalue and eigenvector weighting method introduced in this paper, optimally combining multiple estimates of functional connectivity.

To infer graph communities, we compute the $i$-th eigenvector $\hat{\mathbf{u}}_i$ as a linear combination of the $i$-th eigenvectors of the $K$ Laplacian matrices, using optimally selected weights as specified in (22). We then apply classical spectral clustering [46], performing $k$-means algorithm to first $P$ eigenvectors $\hat{\mathbf{u}}_i$, $i = 1 \cdots P$. This approach yields a robust representation of brain's community structure.

We apply our method to EEG signals recorded during right hand motor imagery and resting state conditions [14]. The results of the community detection are shown in Fig. 16, where panel a) presents results for right-hand motor imagery and panel b) for the resting state condition. Each node is colored according to the community label obtained by optimally merging the $K$ estimates of $A_{\mathcal{C}}^{B_\alpha}$, $A_{\mathcal{IC}}^{B_\alpha}$ and $A_{\mathcal{PD}}^{B_\alpha}$ and considering $P = 5$, as derived from the gap analysis. During resting state, graph communities are diffused and symmetric across the scalp, whereas motor imagery reveals a distinct community in the contralateral motor area (left central).

To incorporate additional trials into the analysis, we build a matrix that captures community organization independently of specific community numbering. We associate each $p$-th community with an $N$-dimensional indicator vector $\mathbf{b}^{(p)}$, where the $n$-th element $\mathbf{b}_n^{(p)} \in \{0, 1\}$ is 1 if node $n$ belongs to the $p$-th community, and 0 otherwise. We then define an $N \times N$ co-association matrix $\Phi$ to indicate whether two nodes belong to the same community. This is computed as:

$$\Phi = \sum_{p=1}^{P} \mathbf{b}^{(p)} \cdot \mathbf{b}^{(p)\,T} \tag{35}$$

The benefit of using the co-association matrix $\Phi$ is that it stays consistent regardless of the order in which communities are labeled, which may vary between experiments.

We evaluate how community-based features differ between two mental states in motor imagery experiments by computing $\Phi$ across multiple trials, and conducting statistical tests to assess the separability between motor imagery and rest conditions. To determine whether differences in $\Phi$ are statistically significant, we perform a t-test, a statistical test that compares the means of two groups to assess if they are significantly different. The discriminative potential of $\Phi$ is evaluated using t-values, which indicate whether each element $\Phi_{m_1 m_2}$ shows a significant difference between the two states.

Specifically, we compute the t-value associated to the difference of the coefficient $\Phi_{m_1 m_2}$, $m_1, m_2 = 1, \cdots N-1$ in the two states, over 100 trials, and for a single subject. The results of the t-test are shown in Fig. 16, panel c). The panel displays t-values associated to the node pair $(m_1, m_2)$ by colored links between the two nodes; the colorbar indicates t-values at a significance level of $\rho = 0.05$, meaning there is a 5% probability that the observed difference occurred by chance. Highlighted links correspond to statistically significant values, meaning that the $m$-th edge between the $m_1, m_2$ nodes shows a significant difference between the motor imagery and rest conditions. In particular, the colored edges are associated with positive t-values, indicating that nodes connected by these edges have a higher probability of grouping together during motor imagery than during rest. This is particularly noteworthy, as the statistically significant region lies in the contralateral left hemisphere. These findings suggest that nodes in this region, already known to be involved in motor imagery tasks [12], change their clustering patterns between the two conditions. Overall, these results emphasize the engagement of contralateral regions during motor imagery tasks and demonstrate a lateralization of activity associated with motor imagery.

To compare the performance of our proposed method with baseline approaches, we consider spectral clustering obtained by averaging Laplacians or directly eigenvectors across $K$ layers. The results shown in Fig. 17(a) and (b) refer to motor imagery and must be compared with Fig. 16(a). Comparing these figures, it appears that baseline methods present poorer community structure: in both cases, we observe one large central community involving most electrodes, and other peripheral communities composed of only few nodes, often in noisy scalp peripheral areas. This differs from the community structure extracted using our method (Fig. 17(a)), which captures spatially coherent and lateralized communities during motor

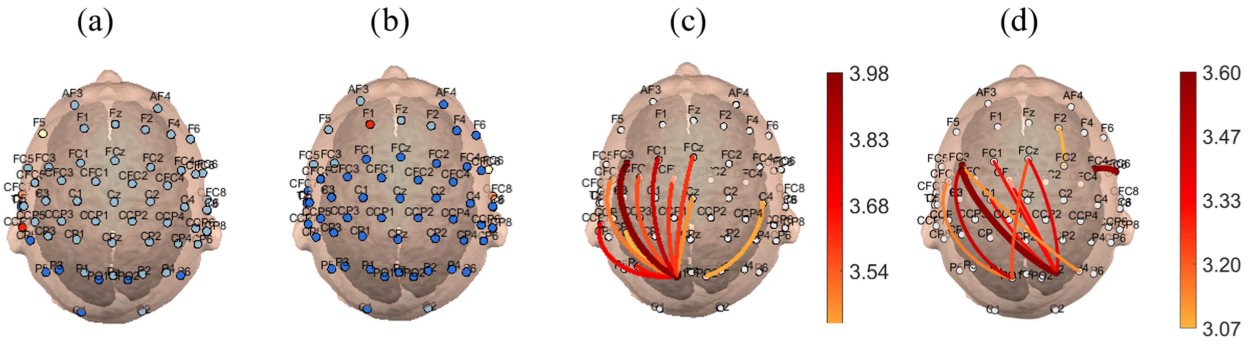


Fig. 17. Community detection results with different averaging strategies on EEG data. Panels (a) and (b) show the communities detected during motor imagery using the average of the Laplacian matrices and the average of the eigenvectors, respectively. Panels (c) and (d) show the results of a t-test on $\Phi$, comparing motor imagery and rest conditions, using the Laplacian mean and eigenvector mean methods, respectively.

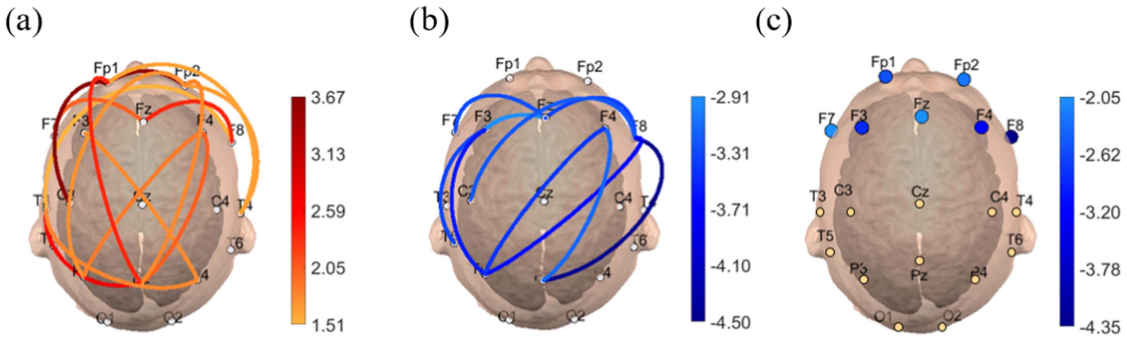


Fig. 18. Graph learning on multiple network estimates $A_{\mathcal{C}}^{B_\theta}$, $A_{\mathcal{C}}^{B_\alpha}$, $A_{\mathcal{C}}^{B_\beta}$ and $A_{\mathcal{C}}^{B_\gamma}$. Panel (a) example of weighted graph obtained from HC subject. Panel (b) results of t-test on $\hat{\mathbf{A}}$ between AD patients and HC subjects. Panel (c) results of the t-test on $\hat{\mathbf{D}}$ between AD patients and HC subjects.

imagery tasks. We also compute the co-association matrix $\Phi$ for each method to perform a t-test on its elements, similarly to our approach in Fig. 16(c). In Fig. 17(c) and (d), we show the statistically significant differences in community structure between motor imagery and resting state using the Laplacian mean and eigenvector mean methods, respectively. Comparing Fig. 17(c) and (d) with Fig. 16(c), the t-values are notably lower compared to those obtained with our method, indicating that our method provides higher discriminatory power. This is confirmed by the spatial location where the changes are observable in the two cases: with the baseline methods, the changes are mostly located in posterior peripheral areas, which are typically less relevant to motor imagery tasks and more affected by noise.

### *E. Brain Graph Learning*

Estimating graph topology is a key aspect in neuroscience research [47]. In this subsection, we explore the potential of our approach, which combines multiple graph estimates to characterize and distinguish brain cognitive states related to the Alzheimer Disease.

Using EEG data from AD patients and healthy control (HC) subjects [15], we extract spectral coherence in $K=4$ frequency bands, treating them as multiple perturbed estimates: $A_{\mathcal{C}}^{B_\theta}$, $A_{\mathcal{C}}^{B_\alpha}$, $A_{\mathcal{C}}^{B_\beta}$ and $A_{\mathcal{C}}^{B_\gamma}$.

The optimally weighted eigenvalues and eigenvectors in (17) and (18) are combined for graph learning purposes, resulting in a new matrix: $\hat{\mathbf{L}} = \hat{\mathbf{U}}\hat{\mathbf{\Lambda}}\hat{\mathbf{U}}^H$. This new matrix is symmetric, semidefinite positive and it has a null eigenvalue by construction. Hence, $\hat{\mathbf{L}}$ retains most of the properties of a Laplacian matrix, but not all. So that we cannot formally say that $\hat{\mathbf{L}}$ is a Laplacian matrix. Following this approach, it is possible to derive a matrix $\hat{\mathbf{A}} = \hat{\mathbf{D}} - \hat{\mathbf{L}}$, that resembles an adjacency matrix, although it does not necessarily contain only non-negative entries. The same applies to the matrix $\hat{\mathbf{D}}$, which is analogous to a degree matrix.

Fig. 18 shows results from graph learning based on the connectivity estimates $A_{\mathcal{C}}^{B_\theta}$, $A_{\mathcal{C}}^{B_\alpha}$, $A_{\mathcal{C}}^{B_\beta}$ and $A_{\mathcal{C}}^{B_\gamma}$. In Fig. 18(a) we display the top 8% strongest links for a control subject. evaluate the discriminative power of graph connectivity, we conduct statistical tests on the learned graph, namely on the adjacency matrix and the node degrees. We run the test across the 60 subjects, half of whom have AD. Fig. 18(b) presents the result of the test on $\hat{\mathbf{A}}$. The t-value for the element $m_1, m_2$ of $\hat{\mathbf{A}}$ is represented as a colored link between the nodes $m_1$, $m_2$, with negative values indicated in the colorbar. In Fig. 18(c), t-values obtained on $\hat{\mathbf{D}}$ are represented by node color. Both tests, contrasting Alzheimer patients with controls subjects, show a decrease in t-values, suggesting reduced connectivity in AD patients compared to HC.

Our findings indicate a significant reduction in overall connectivity in subjects with AD, observable both in specific

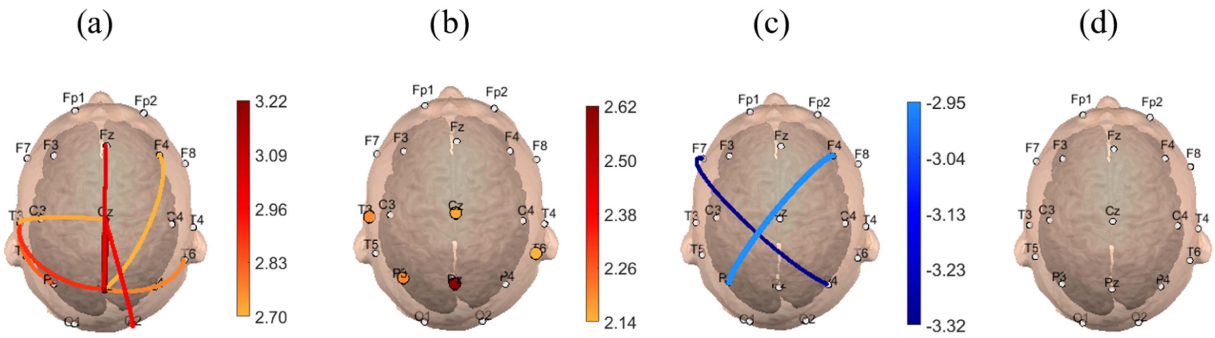


Fig. 19. Results of t-tests between AD and HC. Panel (a) shows the $t$-values computed on the adjacency matrix elements (links) using the average of the Laplacian matrices; panel (b) shows the corresponding $t$-values on node degrees. Panel (c) shows the $t$-values on adjacency matrix entries obtained by averaging the Laplacian eigenvalues and eigenvectors; panel d) shows the corresponding node degree results.

connections and in the broader network structure as measured by node degrees. This connectivity loss may reflect impaired network integration associated with the disease and could serve as a marker for identifying AD.

To compare the performance of our proposed approach with baseline methods, we take into consideration graph learning obtained by i) averaging Laplacians or ii) averaging the eigenvalues and eigenvectors across the $K$ estimates and subsequently reconstructing the Laplacian. We perform statistical tests between AD patients and HC, evaluating both $\hat{\mathbf{A}}$ and $\hat{\mathbf{A}}$ of the learned graphs. Fig. 19(a), (b) show the resulting t-values obtained by averaging the Laplacian matrices, while Fig. 19(c), (d) show the t-values from averaging eigenvalues/eigenvectors. Both the couples of figures have to be compared with Fig. 18(b), (c). Comparing Fig. 19 with Fig. 18(b), (c), we observe that the t-values, both on links and on node degrees, are consistently lower in absolute value with respect to baseline methods. We remark that Fig. 19(d) does not show any significant difference between AD and C. This means that our method is more effective in identifying graph connectivity alterations associated with AD, both at the level of specific connections and at the graph-level, measured by node degree.

## V. Conclusion

This paper presents a robust method to infer the brain graph topology by integrating multiple estimates using statistical priors and small perturbation theory. Our method optimally combines spectral properties of network estimated in multiple trials, by different connectivity estimators, or in various frequency bands, and it captures a comprehensive view of the underlying brain network structure. This framework leverages statistical priors for edge reliability, weighting eigenvalues and eigenvectors to account for variations in network topology, and it offers a measure of functional connectivity under topological uncertainty. Applying this approach to EEG data, we demonstrate its effectiveness in identifying brain community structures and quantifying connectivity changes associated with different mental states, such as motor imagery, as well as disease conditions like Alzheimer's disease. This method facilitates the detection of functional communities and critical connectivity elements, offering deeper insights into the mechanisms underlying cognitive states and their reorganization in response to disease.

## References

[1] A. Ortega, P. Frossard, J. Kovačević, J. M. Moura, and P. Vandergheynst, "Graph signal processing: Overview, challenges, and applications," *Proc. IEEE*, vol. 106, no. 5, pp. 808–828, May 2018.

[2] A. Sandryhaila and J. M. Moura, "Discrete signal processing on graphs," *IEEE Trans. Signal Process.*, vol. 61, no. 7, pp. 1644–1656, Apr. 2013.

[3] T. Cattai, G. Scarano, M.-C. Corsi, F. D. V. Fallani, and S. Colonnese, "Community detection from multiple observations: From product graph model to brain applications," *IEEE Trans. Signal Inf. Process. Netw.*, vol. 11, pp. 201–214, 2025.

[4] W. Huang et al., "A graph signal processing perspective on functional brain imaging," *Proc. IEEE*, vol. 106, no. 5, pp. 868–885, May 2018.

[5] C.-M. Ting, S. B. Samdin, M. Tang, and H. Ombao, "Detecting dynamic community structure in functional brain networks across individuals: A multilayer approach," *IEEE Trans. Med. Imag.*, vol. 40, no. 2, pp. 468–480, Feb. 2021.

[6] A. M. Bastos and J.-M. Schoffelen, "A tutorial review of functional connectivity analysis methods and their interpretational pitfalls," *Front. Syst. Neurosci.*, vol. 9, 2016, Art. no. 175.

[7] J. Guillon et al., "Loss of brain inter-frequency hubs in Alzheimer's disease," *Sci. Rep.*, vol. 7, no. 1, pp. 1–13, 2017.

[8] E. Bayram, D. Thanou, E. Vural, and P. Frossard, "Mask combination of multi-layer graphs for global structure inference," *IEEE Trans. Signal Inf. Process. Netw.*, vol. 6, pp. 394–406, 2020.

[9] P.-Y. Chen and A. O. Hero, "Multilayer spectral graph clustering via convex layer aggregation: Theory and algorithms," *IEEE Trans. Signal Inf. Process. Netw.*, vol. 3, no. 3, pp. 553–567, Sep. 2017.

[10] G. Chao, S. Sun, and J. Bi, "A survey on multiview clustering," *IEEE Trans. Artif. Intell.*, vol. 2, no. 2, pp. 146–168, Apr. 2021.

[11] T. Cattai, G. Scarano, M.-C. Corsi, F. D. V. Fallani, and S. Colonnese, "EEG as signal on graph: A multilayer network model for BCI applications," in *Proc. 30th Eur. Signal Process. Conf.*, 2022, pp. 932–936.

[12] T. Cattai, S. Colonnese, M.-C. Corsi, D. S. Bassett, G. Scarano, and F. D. V. Fallani, "Phase/amplitude synchronization of brain signals during motor imagery BCI tasks," *IEEE Trans. Neural Syst. Rehabil. Eng.*, vol. 29, pp. 1168–1177, 2021.

[13] E. Ceci and S. Barbarossa, "Graph signal processing in the presence of topology uncertainties," *IEEE Trans. Signal Process.*, vol. 68, pp. 1558–1573, 2020.

[14] B. Blankertz, G. Dornhege, M. Krauledat, K.-R. Müller, and G. Curio, "The non-invasive berlin brain–computer interface: Fast acquisition of effective performance in untrained subjects," *NeuroImage*, vol. 37, no. 2, pp. 539–550, 2007.

[15] A. Miltiadous et al., "A dataset of scalp EEG recordings of Alzheimer's disease, frontotemporal dementia and healthy subjects from routine EEG," *Data*, vol. 8, no. 6, 2023, Art. no. 95.

[16] J. H. Wilkinson, *The Algebraic Eigenvalue Problem*. Oxford, U.K.: Oxford Univ. Press, Inc., 1988.

[17] G. W. Stewart, *Introduction to Matrix Computations*. Amsterdam, The Netherlands: Elsevier, 1973.
[18] S. Borjigin and C. Guo, "Perturbation analysis for the normalized laplacian matrices in the multiway spectral clustering method," *Sci. China. Inf. Sci.s*, vol. 57, no. 11, pp. 1–17, 2014.
[19] S. Hata and H. Nakao, "Localization of laplacian eigenvectors on random networks," *Sci. Rep.*, vol. 7, no. 1, 2017, Art. no. 1121.
[20] D. A. Spielman, "Spectral graph theory and its applications," in *Proc. 48th Annu. IEEE Symp. Foundations Comput. Sci.*, 2007, pp. 29–38.
[21] M. Sabbaqi and E. Isufi, "Inferring time varying signals over uncertain graphs," in *Proc. IEEE Int. Conf. Acoust. Speech Signal Process.*, 2024, pp. 9876–9880.
[22] I. Spinelli, S. Scardapane, A. Hussain, and A. Uncini, "FairDrop: Biased edge dropout for enhancing fairness in graph representation learning," *IEEE Trans. Artif. Intell.*, vol. 3, no. 3, pp. 344–354, Jun. 2022.
[23] S. Colonnese, P. D. Lorenzo, T. Cattai, G. Scarano, and F. D. V. Fallani, "A joint markov model for communities, connectivity and signals defined over graphs," *IEEE Signal Process. Lett.*, vol. 27, pp. 1160–1164, 2020.
[24] G. Gordon and R. Tibshirani, "Karush-Kuhn-Tucker conditions," *Optimization*, vol. 10, no. 725/36, 2012, Art. no. 725.
[25] K. Ye and L.-H. Lim, "Schubert varieties and distances between subspaces of different dimensions," *SIAM J. Matrix Anal. Appl.*, vol. 37, no. 3, pp. 1176–1197, 2016.
[26] T. Cattai, "Perturbation-based analysis of brain networks," 2024. Accessed: Apr. 08, 2025. [Online]. Available:https://github.com/TizianaCattai/PerturbationBrainNet
[27] J. Gonzalez-Astudillo, T. Cattai, G. Bassignana, M.-C. Corsi, and F. D. Vico Fallani, "Network-based brain computer interfaces: Principles and applications," *J. Neural Eng.*, vol. 18, 2020, Art. no. 011001.
[28] G. C. Carter, "Coherence and time delay estimation," *Proc. IEEE*, vol. JPROC-75, no. 2, pp. 236–255, Feb. 1987.
[29] G. Nolte, O. Bai, L. Wheaton, Z. Mari, S. Vorbach, and M. Hallett, "Identifying true brain interaction from eeg data using the imaginary part of coherency," *Clin. Neuriophysiol.*, vol. 115, no. 10, pp. 2292–2307, 2004.
[30] H. Yang et al., "Subgroup identification through multiplex community structure within functional connectivity networks," in *Proc. IEEE Int. Conf. Acoust. Speech Signal Process.*, 2024, pp. 2141–2145.
[31] M. Tangermann et al., "Review of the BCI competition IV," *Front. Neurosci.*, vol. 6, 2012, Art. no. 55.
[32] W. Hoeffding, "Probability inequalities for sums of bounded random variables," in *The Collected Works Wassily Hoeffding*, Berlin, Germany: Springer, 1994, pp. 409–426.
[33] J. O. Garcia, A. Ashourvan, S. Muldoon, J. M. Vettel, and D. S. Bassett, "Applications of community detection techniques to brain graphs: Algorithmic considerations and implications for neural function," *Proc. IEEE*, vol. 106, no. 5, pp. 846–867, May 2018.
[34] E. Al-Sharoa, M. Al-Khassaweneh, and S. Aviyente, "Tensor based temporal and multilayer community detection for studying brain dynamics during resting state fMRI," *IEEE Trans. Biomed. Eng.*, vol. 66, no. 3, pp. 695–709, Mar. 2019.
[35] A. Calderone et al., "Comparing alzheimer's and parkinson's diseases networks using graph communities structure," *BMC Syst. Biol.*, vol. 10, pp. 1–10, 2016.
[36] M. S. Yamamoto, K. Sadatnejad, T. Tanaka, R. Islam, Y. Tanaka, and F. Lotte, "Detecting EEG outliers for BCI on the riemannian manifold using spectral clustering," in *Proc. 42nd Annu. Int. Conf. IEEE Eng. Med. Biol. Soc.*, 2020, pp. 438–441.
[37] M. S. Yamamoto et al., "Modeling complex EEG data distribution on the riemannian manifold toward outlier detection and multimodal classification," *IEEE Trans. Biomed. Eng.*, vol. 71, no. 2, pp. 377–387, Feb. 2024.
[38] C. Presigny and F. D. V. Fallani, "Colloquium: Multiscale modeling of brain network organization," *Rev. Modern Phys.*, vol. 94, no. 3, 2022, Art. no. 031002.
[39] U. Herwig, P. Satrapi, and C. Schönfeldt-Lecuona, "Using the international 10-20 EEG system for positioning of transcranial magnetic stimulation," *Brain Topogr.*, vol. 16, pp. 95–99, 2003.
[40] I. Echegoyen, D. López-Sanz, F. Maestú, and J. M. Buldú, "From single layer to multilayer networks in mild cognitive impairment and alzheimer's disease," *J. Phys: Complexity*, vol. 2, no. 4, 2021, Art. no. 045020.
[41] C. Bordier, C. Nicolini, and A. Bifone, "Graph analysis and modularity of brain functional connectivity networks: Searching for the optimal threshold," *Front. Neurosci.*, vol. 11, 2017, Art. no. 441.
[42] G. Marrelec et al., "Partial correlation for functional brain interactivity investigation in functional MRI," *Neuroimage*, vol. 32, no. 1, pp. 228–237, 2006.
[43] F. D. V. Fallani, V. Latora, and M. Chavez, "A topological criterion for filtering information in complex brain networks," *PLoS Comput. Biol.*, vol. 13, no. 1, 2017, Art. no. e1005305.
[44] N. Langer, A. Pedroni, and L. Jäncke, "The problem of thresholding in small-world network analysis," *PLoS One*, vol. 8, no. 1, 2013, Art. no. e53199.
[45] T. Adamovich, I. Zakharov, A. Tabueva, and S. Malykh, "The thresholding problem and variability in the eeg graph network parameters," *Sci. Rep.*, vol. 12, no. 1, 2022, Art. no. 18659.
[46] A. Ng, M. Jordan, and Y. Weiss, "On spectral clustering: Analysis and an algorithm," in *Proc. Adv. Neural Inf. Process. Syst.*, 2001, pp. 849–856.
[47] F. D. V. Fallani, J. Richiardi, M. Chavez, and S. Achard, "Graph analysis of functional brain networks: Practical issues in translational neuroscience," *Philos. Trans. Roy. Soc. B: Biol. Sci.*, vol. 369, no. 1653, 2014, Art. no. 20130521.